Available online at www.CivileJournal.org

Civil Engineering Journal

(E-ISSN: 2476-3055; ISSN: 2676-6957)

Vol. 11, No. 12, December, 2025

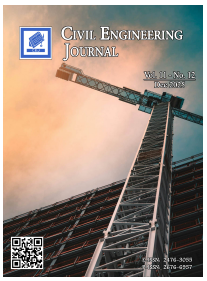

Performance Evaluation of Semi-Precast Reinforced Concrete Slabs Under Flexural Load

Samy Elbialy [1-3*], Doaa Youssef [4], Walid F. Edris [3, 5], Gouda Ghanem [1], Wael Ibrahim [1]

[1] Civil Engineering Department, Faculty of Engineering at Mataria, Helwan University, Cairo 11718, Egypt.

[2] Department of Civil and Environmental Engineering, University of Strathclyde in Bahrain, Harbour Heights, Bahrain.

[3] Department of Civil and Environmental Engineering, College of Engineering and Design, Kingdom University, 40434, Bahrain.

[4] Department of Civil Engineering, Shorouk Academy, The Higher Institute of Engineering, El Shorouk City, Cairo 11837, Egypt.

[5] Department of Civil Engineering, Giza High Institute of Engineering and Technology, Giza 12611, Egypt.

Received 05 September 2025; Revised 15 November 2025; Accepted 22 November 2025; Published 01 December 2025

Abstract

This study aims to evaluate the flexural performance of semi-precast reinforced concrete slabs incorporating steel lattice girders as internal reinforcement. The objective is to investigate the influence of geometric and material parameters such as precast slab thickness, lattice girder height, top chord diameter, concrete compressive strength, and the addition of steel or glass fibers on overall flexural capacity and deformation behavior. Thus, previous studies have shown that replacing conventional cast-in-situ slabs with semi-precast systems can reduce total construction costs by 43–70%. Thirteen semi-precast slabs and one control slab were tested under four-point bending, and a nonlinear finite element model was developed in ABAQUS to simulate the experimental response. The analysis focused on load–deflection behavior, strain distribution, and failure modes. Results indicated that increasing slab thickness and chord diameter enhanced stiffness and load-bearing capacity, while higher concrete strength and fiber reinforcement improved crack control and reduced deflection. The FEM model demonstrated strong agreement with experimental results, validating its reliability for predicting structural performance. This study extends previous research by integrating a broad experimental parameter range with a validated ABAQUS finite element model, providing new insights into the structural optimization and cost efficiency of semi-precast slab systems. The proposed semi-precast system exhibited ductile behavior and achieved savings in formwork and labor cost compared with conventional flat slabs, offering a practical and sustainable alternative for efficient concrete construction.

Keywords: Semi Precast Slab; Abaqus Software; Steel, Glass Fiber; Flexural Performance; Stress Distribution; Crack Pattern.

1. Introduction

Reinforced concrete (RC) remains one of the most widely used construction materials due to its strength, durability, and adaptability. However, traditional RC construction depends heavily on temporary wooden or steel formwork, which increases material and labor costs, prolongs construction schedules, and generates significant waste. To improve sustainability and productivity, precast concrete systems have been developed to reduce on-site labor, enhance quality control, and minimize environmental impact [1, 2]. The adoption of precast systems has gained momentum in medium- and high-rise buildings, offering time savings, cost efficiency, and improved safety [3, 4]. Despite these advantages,

* Corresponding author: samy.elbialy@strath.ac.uk

http://dx.doi.org/10.28991/CEJ-2025-011-12-07

© 2025 by the authors. Licensee C.E.J, Tehran, Iran. This article is an open access article distributed under the terms and conditions of the Creative Commons Attribution (CC-BY) license (http://creativecommons.org/licenses/by/4.0/).

fully precast slabs often present challenges in transportation, lifting, and alignment due to their weight. Consequently, semi-precast slab systems, which combine precast base elements with cast-in-place concrete toppings, have emerged as a more practical and lightweight alternative. These systems serve both as permanent formwork and as structural components, achieving full composite action after the cast-in-place concrete hardens. Previous studies have shown that replacing conventional cast-in-situ slabs with semi-precast systems can reduce total construction costs by 43–70 % [5, 6]. A key feature of semi-precast slabs is the steel lattice girder, which significantly enhances load transfer and flexural stiffness. These girders form a three-dimensional framework composed of an upper chord, two lower chords, and diagonal braces connected by resistance welding. During construction, the lattice girder provides temporary rigidity until the in-situ concrete achieves full strength, allowing the system to act compositely [7].

Several researchers have examined the influence of geometric parameters on the performance of such slabs. Zhang et al. [8] investigated allowable spans for lattice-girder-reinforced semi-precast slabs and confirmed their structural efficiency. Hillebrand et al. [9] demonstrated that lattice girders improve stiffness, load-sharing, and reduce mid-span deflection, outperforming flat reinforcement systems due to better interfacial bonding between the precast and topping layers. Löfgren [10] optimized lattice girder height and spacing to improve stress distribution and bending resistance, while Xu et al. [11] investigated the fire performance of semi-precast slabs, confirming adequate resistance exceeding 130 minutes. Other studies have focused on the interface behavior and long-term composite action between precast and cast-in-place concrete. Lam et al. [12] defined a minimum bond strength of approximately 1 MPa as the threshold for achieving full composite performance. Mohamed et al. [13] experimentally demonstrated that increasing surface roughness and mechanical interlock significantly enhances interface shear capacity and delays debonding between the precast and cast-in-place layers, while Baran [14] reported limited composite action at high load levels due to interface slip. Adawi et al. [15] developed a nonlinear finite element model to simulate interfacial shear transfer and post-cracking behavior. More recently, Hillebrand et al. [9, 16] investigated the shear and interface shear fatigue behavior of semi-precast slabs with lattice girders, confirming that the lattice system provides reliable shear transfer and maintains composite action under cyclic loading. Recent research has also focused on fiber-reinforced and hybrid semi-precast systems.

Mahmoud et al. [17] examined eight full-scale slabs and found that incorporating steel, chopped basalt, or basalt minibar fibers in the bottom layer significantly enhanced flexural capacity and crack control. Rahimi Mansour et al. [18] highlighted the roles of surface roughness and fiber-reinforced toppings in improving ductility and crack control. As a comparison, previous studies have demonstrated that using steel reinforcement in ribbed slab systems offers high load-carrying capacity and stiffness [19-21]. On the other hand, fiber-reinforced materials often face limitations in terms of availability and long-term performance under structural conditions [22, 23]. More recent efforts have focused on numerical modeling and design optimization. Newell et al. [24] monitored semi-precast floor slabs during construction and service stages to assess structural behavior. The measured deflections validated their finite element model, confirming effective composite action and accurate FEM prediction under service loads, while Zhang et al. [25] experimentally and numerically studied precast insulation mortar sandwich panels with truss-shaped steel shear connectors. The results confirmed effective shear transfer and flexural stiffness, showing close agreement between FEM and experimental outcomes.

Yun et al. [26] proposed a Euler–Bernoulli beam theory–based sectional analysis method for predicting the effective stiffness of lattice girder composite slabs (LGCS), allowing for rapid estimation of second moments of area without relying solely on finite element models. His study compared analytical predictions with experimental and FE-based results, confirming the model's ability to capture stiffness variations due to changes in girder geometry and material properties. Despite these advancements, several research gaps remain. Most previous studies have investigated only single variables, such as lattice girder height or fiber type, without conducting a systematic, multi-parameter evaluation. Limited experimental data exist on how geometric configurations and material properties jointly influence the flexural performance of semi-precast slabs. Moreover, few studies have validated experimental findings through detailed finite element modeling that explicitly captures stress transfer, cracking progression, and interface behavior between the precast and cast-in-place layers. Therefore, this study aims to fill these gaps by conducting a comprehensive experimental and numerical investigation on the flexural behavior of semi-precast reinforced concrete slabs. Thirteen semi-precast slabs and one control flat slab were tested under four-point bending, examining the effects of lattice girder height, top chord diameter, precast slab thickness, concrete compressive strength, and topping reinforcement type (steel bars, steel fibers, glass fibers). Finite element analysis using ABAQUS was employed to simulate the experiments and evaluate stress distribution, failure modes, and strain development. The novelty of this research lies in its broad parameter range, dual experimental–new numerical validation, and quantitative comparison of different reinforcement configurations, providing new insight into optimizing semi-precast slab systems for both structural and economic efficiency.

2. Research Methodology

This study adopts a sequential methodology, as illustrated in Figure 1. The subsequent sections provide a detailed explanation of each step in the process.

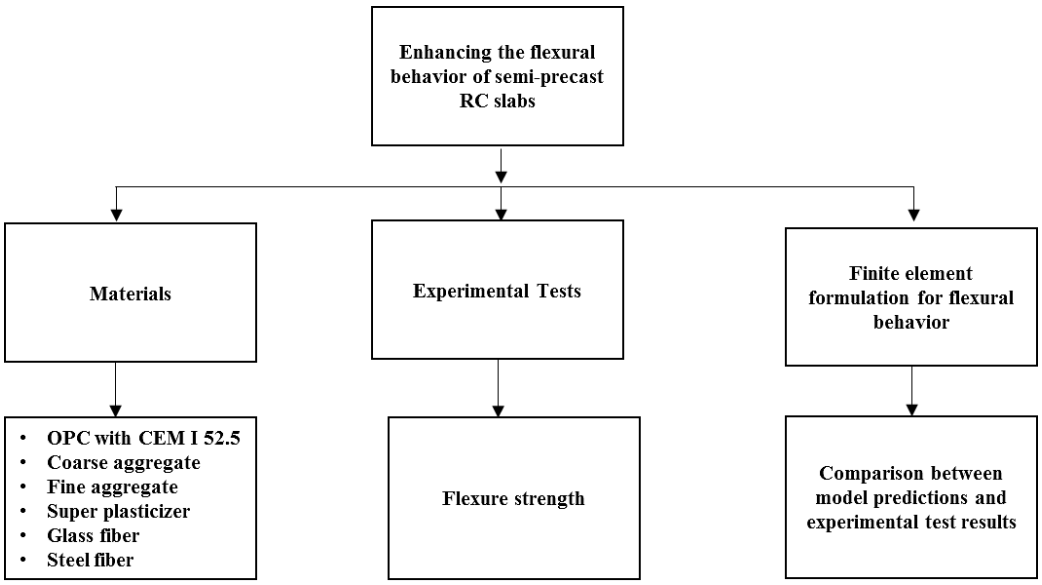

Figure 1. The flowchart of the methodology

3. Selection of Materials

3.1. Aggregate

For the concrete utilized in this study, crushed stone (dolomite) with a maximum particle size of 20 mm served as the coarse aggregate. Natural sand, the fine aggregate, is used. The bulk density of the sand was 2.50, and that of the dolomite was 2.70. A sieve analysis was carried out for both aggregates in accordance with ASTM standards, and the results are presented in Figure 2. The grading curves confirm that both the fine and coarse aggregates complied with the specified limits of ASTM C33M [27], ensuring their suitability for concrete production.

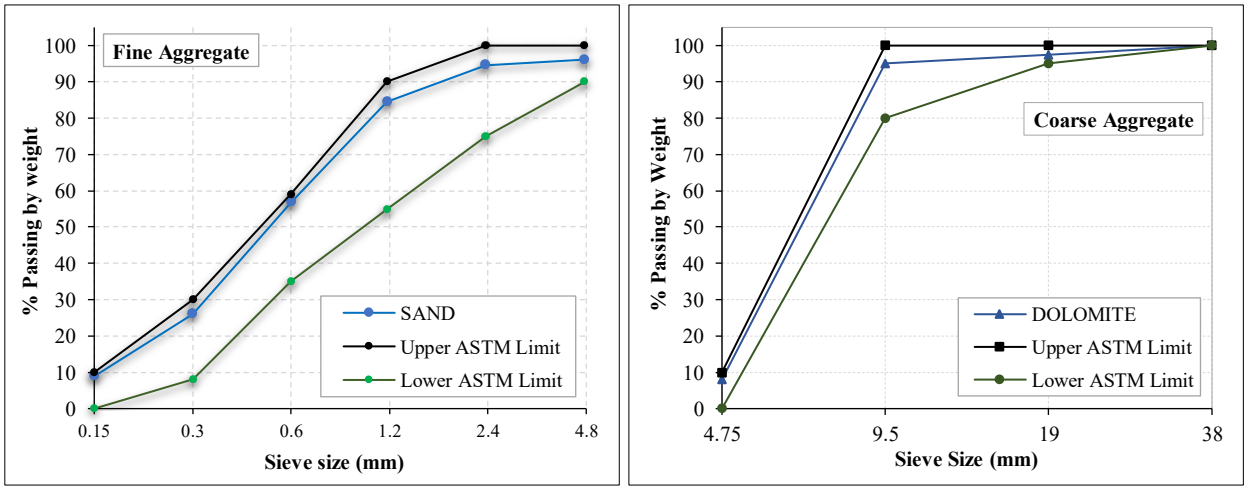

Figure 2. Sieve analysis of coarse and fine aggregates: (Upper and lower limits according to ASTM C 33)

3.2. Cementitious Materials

Concrete mixes were produced using Ordinary Portland Cement (OPC), specifically CEM I 52.5N, as the primary binder. This cement type complies with the requirements of ES 4756-1 [28] and EN 197-1 [29], and was supplied by Helwan Cement Company, Egypt. To improve the mechanical properties of the mixes, silica fume (micro-silica) was incorporated as a supplementary cementitious material. As specified in ASTM C-1240 [30], the silica fume used in this study is a fine gray powder with an average particle size of 0.2 µm, a surface area of approximately 14 m^2/g, and a density of 20 kN/m^3.

3.3. Reinforcement Bars

High-strength steel reinforcement bars of grade 52 were utilized. The bars were produced in various diameters of 10, 12, 16, 18, and 22 mm. Their mechanical properties include a Young's modulus of 200,000 N/mm^2, a yield strain of 0.002, and a density of 78 kN/m^3. The corresponding unit weights for these diameters were 6.17, 8.88, 15.6, 19.9, and 29.8 N/m, respectively. The material exhibited a yield stress of 420 MPa and an ultimate tensile strength of 600 MPa.

3.4. Steel Fiber

The corrugated steel fibers used in this study are illustrated in Figure 3. Their distinctive geometry enables random orientation within the concrete matrix, thereby enhancing stress distribution and promoting more uniform strain transfer. This characteristic contributes to improved crack control and greater load-carrying efficiency of the composite material. The fibers possess a tensile strength of 1250 MPa, which exceeds that of conventional straight steel fibers, further enhancing the mechanical performance of the mix.

Figure 3. Corrugated Steel fiber

3.5. Glass Fiber

Glass fibers as shown in Figure 4, with a length of 18 mm, were used in specimen **S13** to enhance crack resistance and improve durability. The fibers were uniformly distributed in the concrete mixture. Glass fibers provide additional corrosion resistance compared to traditional steel reinforcement, making them ideal for slabs exposed to aggressive environments where corrosion of steel reinforcement might occur. They also help in improving crack control while maintaining the slab's overall strength and performance.

Figure 4. Glass fiber

4. Experimental Work

4.1. Laboratory Specimens

To enhance comprehension of the semi-precast slab's behavior, a total of thirteen semi-precast reinforced concrete one-way slabs and a control flat slab (**FS28**) were constructed and examined under four-point out-of-plane loading. For group (A), consisting of three specimens, the investigating parameter was the different precast slab thicknesses (60, 80, and 100 mm, respectively). For group (B), consisting of two specimens, the investigating parameter was lattice girder height (280 and 300 mm). In group (C) of three specimens, the investigating parameter was top chord diameter (12, 18, and 22). The selected parameters, including top-chord diameters, slab thicknesses, and lattice girder height, were based on practical construction ranges reported in earlier studies and industry guidelines [8, 10]. These values also align with optimization limits that balance strength, weight, and constructability for semi-precast floor systems. For group (D), consisting of two specimens, the investigating parameter was compressive strength (25 and 45) MPa, as shown in Table 1. For group (E), a full-scale slab of thickness 280 mm, as shown in Table 2, consisting of three specimens, the investigating parameter was the cast-in-situ reinforcement (steel bars, steel fiber, and glass fiber), were cast in two layers and a control flat slab. All slabs measured 2400 mm in length and 300 mm in breadth. The study examined the load versus mid-span deflection relationships, crack patterns, failure modes, and the distribution of rebar strains in the specimens.

Table 1. Description of laboratory specimens

GROUP	Slab codes	Precast Slab thickness (mm)	Total slab depth (mm)	Truss height (mm)	Top chord diam. (mm)	Fcu (MPa)
A	S1	60	280	240	16	35
	S2	80	280	240	16	35
	S3	100	280	240	16	35
B	S4	60	320	280	16	35
	S5	60	340	300	16	35
C	S6	60	280	240	22	35
	S7	60	280	240	18	35
	S8	60	280	240	12	35
D	S9	60	280	240	16	25
	S10	60	280	240	16	45

Table 2. Specifications of Full-Thickness Semi-Precast Reinforced Concrete Slabs

GROUP	Slab codes	Span (mm)	Breadth (mm)	Precast Slab depth (mm)	Total slab thickness (mm)	Top reinforcement cast in-situ slab
E	S11	2400	300	60	280	Steel bars
	S12	2400	300	60	280	Steel fiber
	S13	2400	300	60	280	Glass fiber
	FS28	2400	300	60	280	-

4.2. Mix Design

All concrete mixtures were designed according to ACI 211.1 [31]; a concrete mix was designed using coarse aggregate, sand, cement, and water. Table 3 presents five different concrete mixes. The target compressive strength for all mixtures was set at 35 MPa, with the exception of S9, which was designed for 25 MPa, and S10, which was designed for 45 MPa. All mixes had a water-cement ratio (w/c %) of 0.45, except for S9, which had a ratio of 0.5, and S10, which had a ratio of 0.40. Additionally, for S12, a cast-in-situ topping slab incorporated 300 N/m³ of steel fiber (CSF), while for S13; the topping slab included 300 N/m³ of glass fiber (CGF).

Table 3. Quantities of materials for concrete mixtures

Mix Name	Cement (N)	Silica fume (N)	Water (N)	W/C ratio	Aggregate (N)		Steel fiber (N)	Glass fiber (N)
					Coarse	Fine		
C25	3500	-	1750	0.50	12400	6200	-	-
C35	4500	700	2025	0.45	11570	5780	-	-
C45	4700	700	1880	0.40	11570	5780	-	-
CSF	4500	-	2025	0.45	11570	5780	300	-
CGF	4500	-	2025	0.45	11570	5780	-	300

4.3. Casting and Curing Test Specimens

For each concrete mixture, six standard cubes with dimensions of 150 × 150 × 150 mm were prepared to determine the compressive strength (f_{cu}), as illustrated in Figure 5. Three cubes were tested after 7 days, and the remaining three after 28 days under compression at room temperature. The results were compared with those of the control cubes tested at 28 days. In addition, the splitting tensile strength of each mixture was evaluated using three standard cylinders measuring 150 mm in diameter and 300 mm in height.

A total of thirteen slab specimens and a control flat slab were fabricated and tested to evaluate the flexural strength of semi-precast reinforced concrete slabs with and without fibers. All the slabs were 300 mm wide and 2400 mm long, with thicknesses of 60, except S2 and S3 is 80 mm and 100 mm respectively (as shown in Figure 6).

Figure 5. Standard concrete cubes after casting

Figure 6. Reinforcement and casting of slabs

4.4. Test Setup and Instrumentation

Each specimen underwent testing using a four-point bending method. To measure the deflection, Linear Variable Displacement Transducers (LVDTs) were placed at the midpoint and the two loading positions. A hydraulic jack was used to apply the force. Strain gauges were affixed to monitor the strain in the longitudinal reinforcement of the precast slab. The layout of the testing apparatus and a photograph of the setup are provided in Figure 7. Crack propagation is visually observed during testing, and the tested specimen's surface was marked with the locations of the cracks.

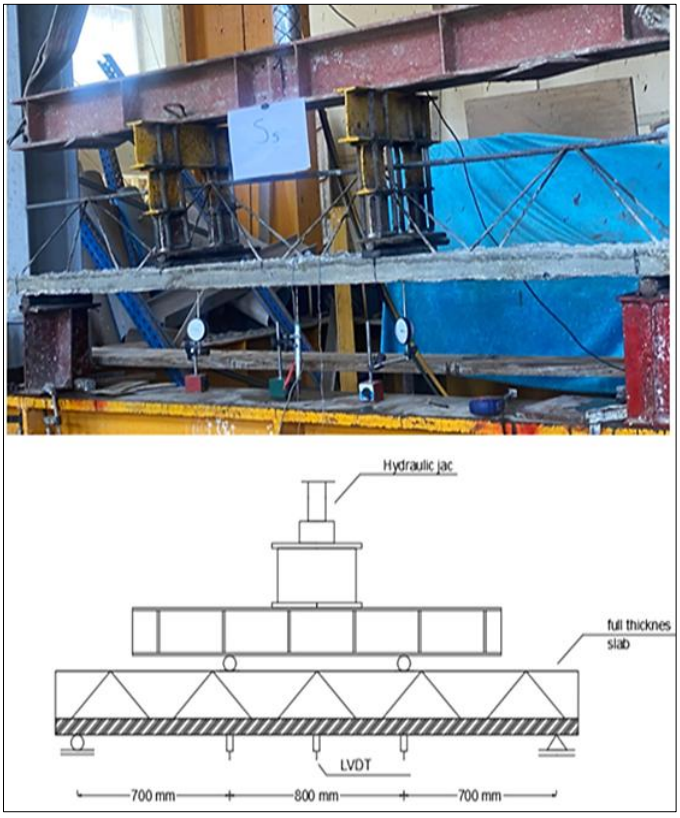

Figure 7. The configuration of the test setup

5. Results and Discussion

5.1. Failure Modes

The typical failure modes of the tested slabs are shown in Figures 8 and 9. Mainly, two types of failure were detected. Failure mode (1) occurred due to the failure of the top-chord bar, as shown in Figure 8. This happened when the top-chord bar diameter was less than or equal to 16 mm, caused by in-plane buckling that increased with the loading rate during testing. The in-plane buckling in the top-chord bar developed under the applied compression load, and bars of 12 mm diameter exhibited a larger value of in-plane deformation before failure. This behavior can be attributed to the high slenderness of the top-chord bars, which makes them more susceptible to elastic instability once the compressive stress exceeds the critical buckling limit. Failure mode (2) was due to the failure of the stirrup welding, as shown in Figure 9. This type of failure occurred directly at the stirrup welding joints within the maximum shear zone of the specimen. It appeared in slabs with top-chord bar diameters greater than 16 mm. This failure was primarily caused by the high shear force transferred through the welds at the support, leading to localized stress concentration and eventual rupture of the weld metal. No deformations or buckling under compression were observed in the top-chord bar for the larger diameters; however, noticeable deformations were observed in the lattice girder stirrups at the maximum shear zone. The failure occurred due to weld fracture under shear load, which may also be related to the presence of heat-affected zones (HAZ) around the welds, where local softening reduces strength and ductility. Also, the good connection between failure modes and mechanical reasoning was observed (buckling vs. welding failure), increasing the buckling significantly increasing the welding failure. The cracking load, failure load, and failure modes of the semi-precast slabs are summarized in Table 4. The cracking and failure loads of full-thickness semi-precast slabs and the control flat slab are shown in Table 5.

Figure 8. Top-Chord Bar Buckling in Semi-Precast Slab with 12 mm bar diameter

Figure 9. Stirrups Welding Failure in Semi-Precast Slab with 22 mm bar diameter

Table 4. Cracking and Failure Load of One-Way Semi-Precast Slabs

GROUP	Slab codes	Cracking Load (kN)	Failure Load (kN)	Type of failure
A	S1	8.82	17.54	Type I
	S2	15.33	19.69	
	S3	21.90	26.50	
B	S4	12.37	14.23	Type I
	S5	6.98	11.80	
C	S6	15.60	21	Type II
	S7	14.10	19.20	
	S8	8.58	12.12	Type I
D	S9	11.60	15.30	Type I
	S10	18.50	20.10	

Table 5. Cracking and Failure Load o Full-Thickness Semi-Precast Slabs

GROUP	Slab codes	Slab thickness	Slab RFT	Cracking Load (kN)	Failure Load (kN)
E	S11	280	Steel bars	86.50	127
	S12	280	Steel fiber	52.80	100
	S13	280	Glass fiber	53.80	118
	Control Slab FS28	280	Upper and lower mesh	78.70	130

5.2. Measured Strain Response

Another perspective on the debonding mechanism can be gained by analyzing the longitudinal tensile strains in both the reinforcing steel and the surrounding concrete. Figures 10 and 11 present the recorded strain values at the crack initiator location corresponding to the yield load and ultimate capacity. Measurements were recorded at the midpoint of the lower reinforcement steel in the semi-precast slabs. The following load-strain chart in Figure 10 shows a comparison between the semi-precast slabs with the different top chord bar and, height of truss, compressive strength, and different thicknesses of semi-precast slab. In group (A), (S3) recorded a higher strain than (S1) at the failure load. For group (B), (S5) recorded a higher strain than (S1). According to Figure 10, at the same loading range on a semi-precast slab with lattice girder reinforcement and the same lattice girder height, the strain in the longitudinal steel reinforcement reduced as the bar diameter increased. Increasing compressive strength in (S10) decreases the strain values.

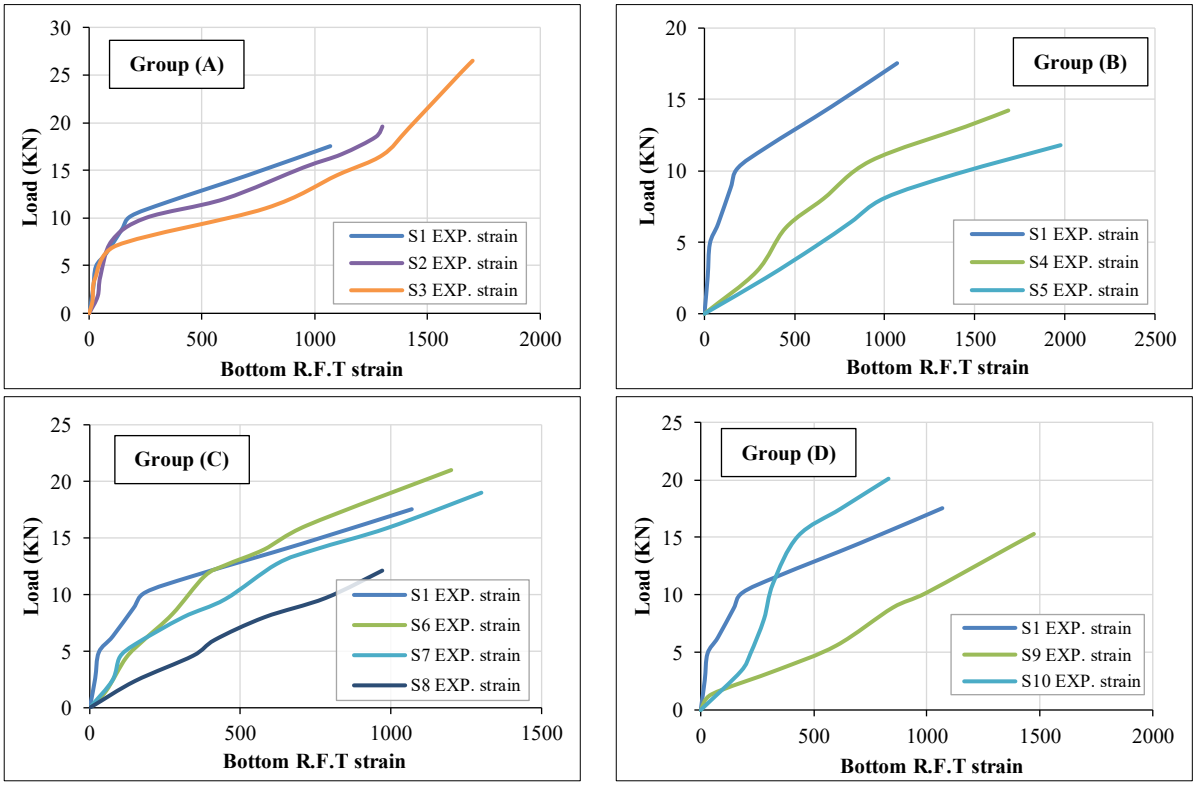

Figure 10. Load-Strain Curves of Semi-Precast Slabs (Groups A–D)

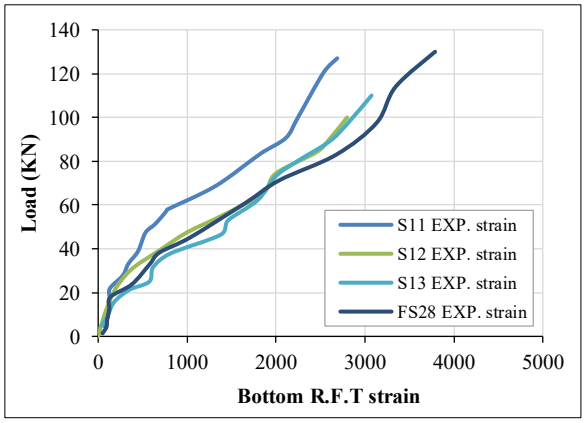

Figure 11. Load-Strain Behavior of Group E Semi-Precast and Control Slabs

The following load-strain curve, Figure 11 shows a comparison between the four slabs with the same thickness of 280 mm. Control flat slab (FS28) recorded a higher strain value than the semi-precast slab at the failure load, which clarifies the effect of the existing steel lattice girder in specimens (S11, S12, and S13), while the bottom bar records lower strain values, the lattice girder truss action reduces the stresses applied in the bottom chord bars because of the connection between truss members that distributes the stresses to all the truss members.

5.3. Crack Pattern of Semi-Precast Slabs and Control Slab (FS28)

Figure 12 presents the observed crack patterns and failure modes of the tested specimens. At the early stages of loading, the slabs showed minimal visible damage. As the load approached the cracking threshold, an initial crack emerged beneath the slab near the mid-span. With continued loading, this crack propagated upward toward the top surface, gradually widening. Concurrently, another crack formed directly beneath the load application point. As loading progressed further, multiple cracks appeared in the constant moment zone, and additional cracking developed in the shear span areas. For specimen S11, cracking initiated at 87.5 kN, with ultimate failure occurring at 127 kN. In contrast, specimen FS28, without steel truss reinforcement, exhibited an early crack at the interface between the precast and cast-in-place concrete layers when the load reached 78.71 kN with ultimate failure 130 kN.

Specimen (S11)

Specimen (S12)

Specimen (S13)

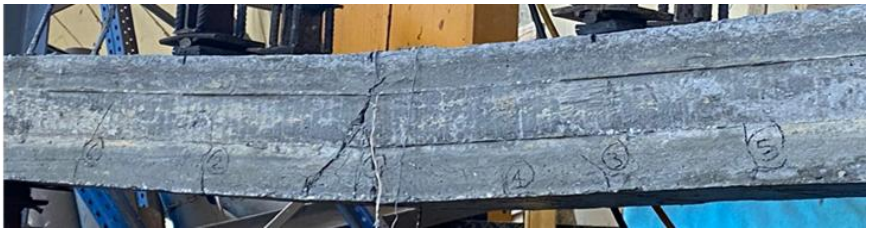

Specimen (FS28)

Figure 12. Crack pattern of full-thickness slab group (E)

5.4. Effect of Precast Slab Thickness

The load–deflection curves (Figure 13-A) show that increasing the precast slab thickness enhanced both stiffness and load capacity. The 100 mm thick slab (S3) carried the highest ultimate load, approximately 26.5 kN (51.08% increase from S1), with the steepest initial slope, followed by the 80 mm slab (S2), while the 60 mm slab (S1) showed the lowest performance. Thicker slabs also exhibited smaller deflections at comparable loads, indicating improved flexural rigidity.

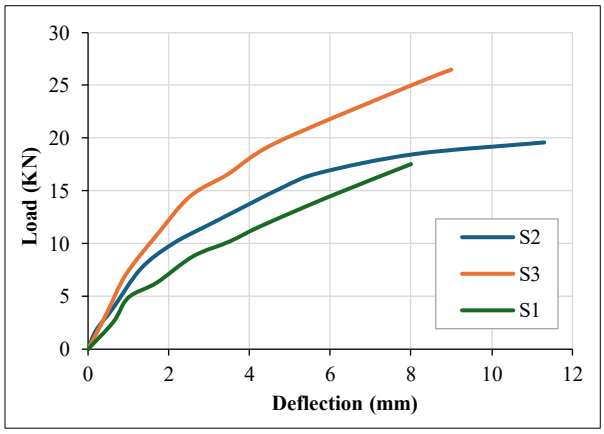

(Group A)

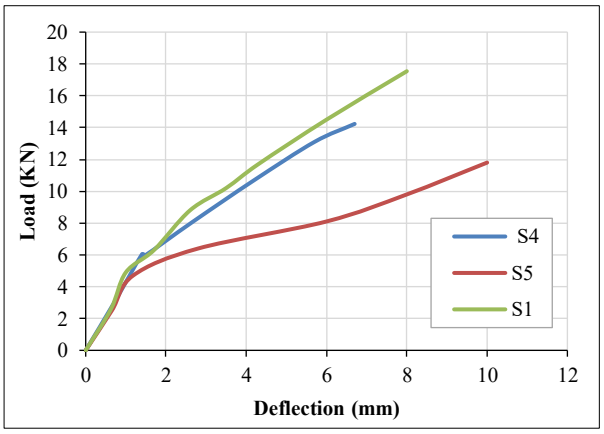

(Group B)

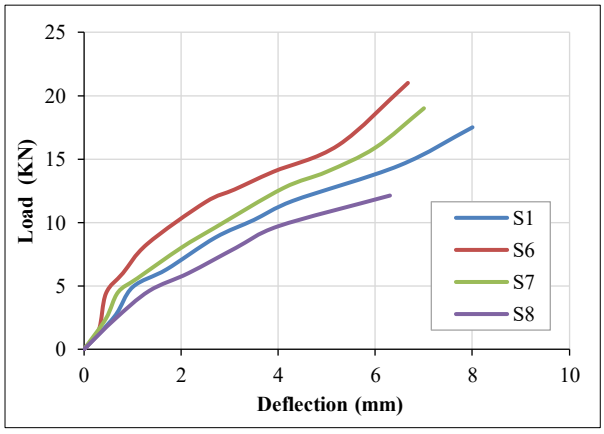

(Group C)

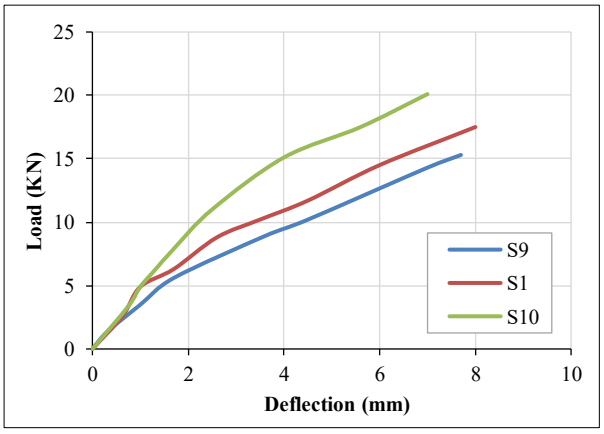

(Group D)

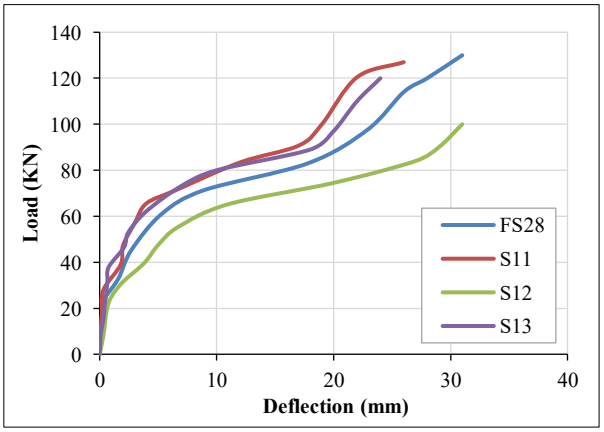

(Group E)

Figure 13. Load-Deflection Comparison of Group (A-E)

5.5. Effect of Lattice Girder Height

The load–deflection curves (Figure 13-B) indicate that increasing the lattice girder height reduced slab deflection and increased stiffness. The 300 mm girder (S5) demonstrated the lowest deflections for a given load, followed by the 280 mm (S4) and 240 mm (S1) girders. While ultimate load capacity varied slightly, the higher girders improved serviceability performance by enhancing flexural rigidity.

5.6. Effect of Top Chord Diameter

The load–deflection curves (Figure 13-C) show that increasing the top chord diameter significantly improved load capacity and stiffness. The 22 mm bar (S6) achieved the highest ultimate load of 21 kN (19.7% increase from S1) and a decrease in deflection to 6.67 mm, followed by the 18 mm (S7), 16 mm (S1), and 12 mm (S8) bars. Larger diameters enhanced tensile resistance in the top chord, delaying yielding and reducing mid-span deflection.

5.7. Effect of Concrete Compressive Strength

The load–deflection curves (Figure 13-D) demonstrate that higher concrete compressive strength leads to increased load capacity and reduced deflection. The slab with 45 MPa concrete (S10) exhibited the highest stiffness and ultimate load followed by the 35 MPa (S1) and 25 MPa (S9) specimens. Decreasing the compressive strength of concrete to 25 MPa in (S10) led to a decrease in failure load to 15.3 kN (14.64% less than S1) with a deflection of 8 mm. Higher-strength concrete improved the compression zone's resistance, delaying crack propagation and reducing deformation, while lower-strength concrete resulted in earlier cracking and greater deflections.

5.8. Effect of Steel and Glass Fiber

The following load-deflection chart (Figure 13-E) compares the performance of four slabs with the same thickness (280 mm) but different reinforcement configurations: a steel truss semi-precast slab, a control flat slab, a steel truss semi-precast slab with steel fiber concrete cast on-site, and a steel truss semi-precast slab with glass fiber concrete cast on-site. This demonstrates that the presence of the steel lattice girder in the semi-precast slab helps reduce deflection when compared to the traditional flat slab, despite both reaching similar failure loads. The S13 semi-precast slab exhibited the lowest deflection at failure load, indicating the beneficial role of glass fibers in improving the slab's ability to resist bending and cracking. The ultimate failure load of the steel fiber slab was 100 kN, while the glass fiber slab reached 118 kN, representing an 18% increase in capacity. The use of glass fibers provides additional crack control and enhances the overall performance of the slab under load, contributing to improved stiffness. The S12 slab also showed improved crack resistance and stiffness compared to the plain S11 slab, but the performance was slightly lower than the **S13** slab in terms of deflection at failure. This suggests that while steel fibers increase the load-bearing capacity and crack resistance, glass fibers may offer better overall performance in reducing deflection due to their larger volume, better distribution, and crack-controlling properties.

6. Finite Element Analysis

6.1. Ultimate and Cracking Load

The finite element modeling was carried out using ABAQUS/Standard (2022) to simulate the flexural behavior of the 13 semi-precast slabs. The concrete material was modeled using the Concrete Damaged Plasticity (CDP) model, which accounts for cracking and crushing nonlinearities. Different concrete grades (f_{cu} = 35–45 MPa) were defined based on the experimental mix properties. Reinforcement bars were modeled as embedded truss elements, as shown in Figure 14. The interface between the precast and cast-in-place layers was modeled using a surface-based cohesive interaction to simulate bond-slip behavior and shear transfer across the interface. Tables 6 and 7, and Figure 15 compare the failure loads obtained from the experimental tests with those predicted by the Abaqus finite element model. The failure load values obtained from the experimental tests and the Abaqus simulations were relatively close for most of the slabs, showing that the finite element model provided a good approximation of the actual structural behavior. In most cases, the failure loads predicted by Abaqus were within a reasonable margin (0-15%) of the experimental values. The S2 and S10 recorded a higher ultimate load with a margin of 14% and 15% in the ABAQUS model than in the experimental program. The comparison between experimental and Abaqus failure load results revealed that the finite element model provided an accurate prediction of the failure load for the semi-precast slabs.

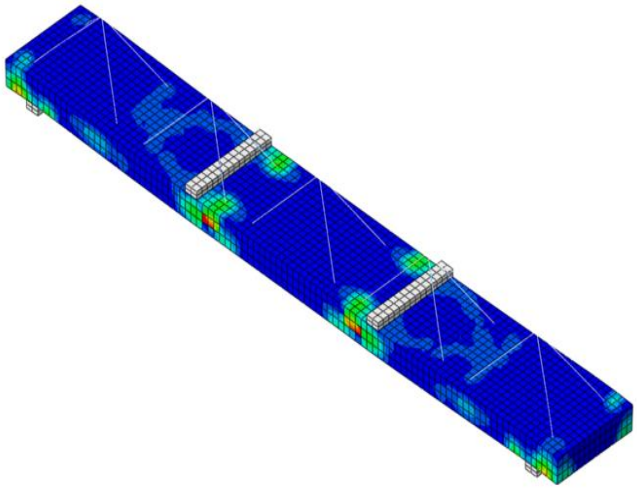

Figure 14. Finite element simulation of semi-precast slab under flexural loading

Table 6. Cracking load, Ultimate Experimental Load and ABAQUS Ultimate Load

GROUP	Slab codes	Cracking Load (KN)	Exp. ultimate load (KN)	Abaqus ultimate load (KN)	Abaqus. Error (KN)	Error (%)
A	S1	8.82	17.54	17.27	0.27	1.54%
	S2	15.33	19.69	22.31	2.62	13.30%
	S3	21.90	26.50	28.20	1.7	6.42%
B	S4	12.37	14.23	12.21	2.02	14.19%
	S5	6.98	11.80	11.75	0.05	0.42%
C	S6	15.60	20.10	22.56	2.46	12.23%
	S7	14.10	19.20	19.48	0.28	1.46%
	S8	8.58	12.12	11.85	0.27	2.23%
D	S9	11.60	15.30	15.13	0.17	1.11%
	S10	18.50	20.10	23.1	3	14.9%

Table 7. Cracking load, Failure Experimental Load and ABAQUS Ultimate Load

GROUP	Slab codes	Cast-in-situ RC slab (RFT)	Cracking Load (KN)	Exp. ultimate load (KN)	Abaqus ultimate load (KN)	Abaqus. Error (KN)	Error (%)
E	S11	Steel bars	86.50	127	130.00	3	2.36%
	S12	Steel fiber	52.80	100	106.48	6.48	6.48%
	S13	Glass fiber	53.79	118	122.97	4.97	4.21%
	Control slab	Upper and lower mesh	78.71	130	117.60	12.4	9.5%

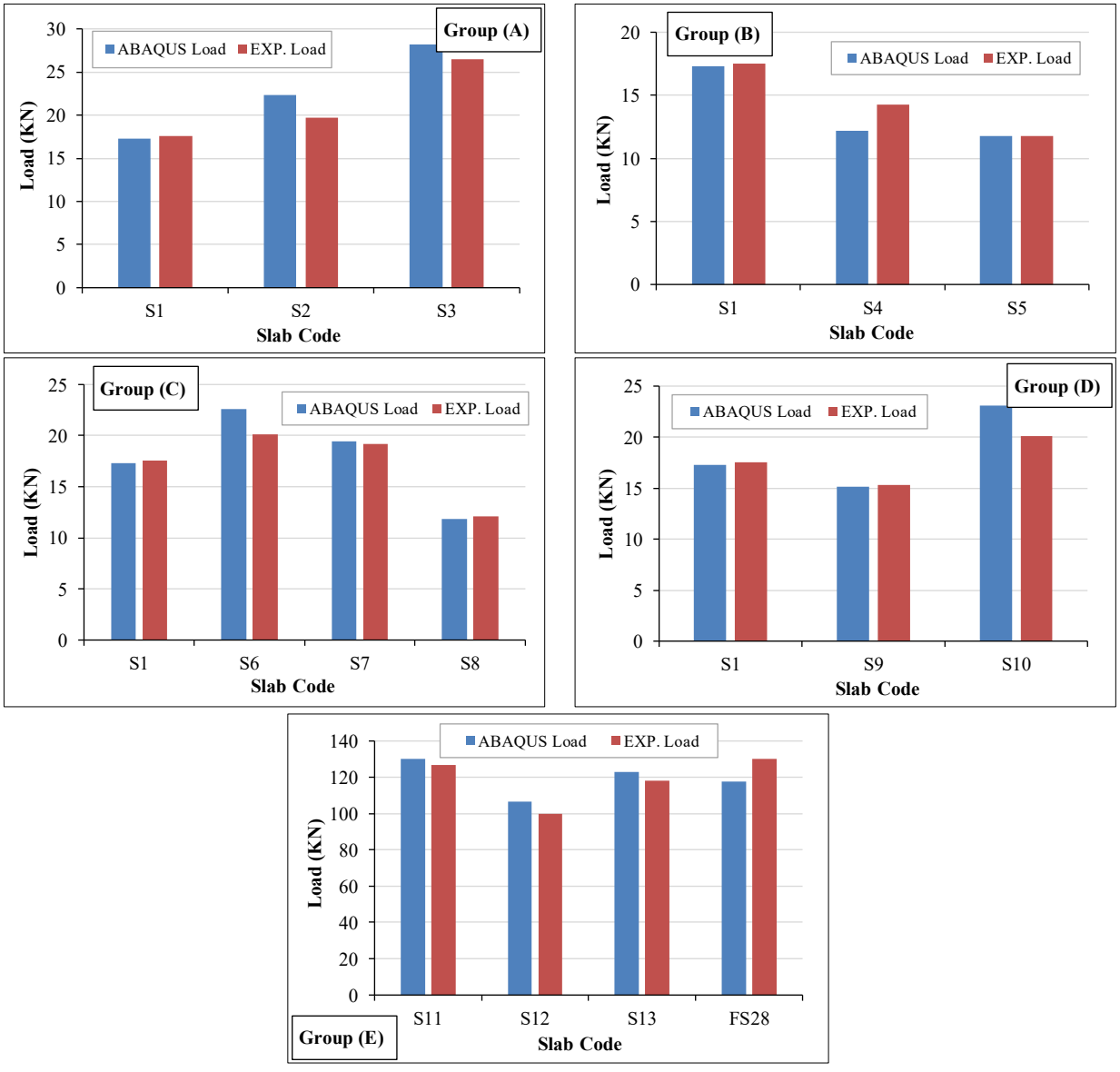

Figure 15. The Failure Load values obtained from the experimental tests and the Abaqus simulation

6.2. Effect of Precast Slab Thickness

Experimental and numerical results indicate that increasing the precast thickness significantly enhances slab stiffness and ultimate load capacity (Figure 16-A). The thickest slab (S3) achieved the highest failure load and exhibited the smallest deflection for the same load level, followed by S2, while S1 showed the lowest stiffness and earliest yielding. The FEM curves closely followed the experimental trends, particularly in the elastic range, with minor deviations observed near peak load due to post-cracking nonlinearities.

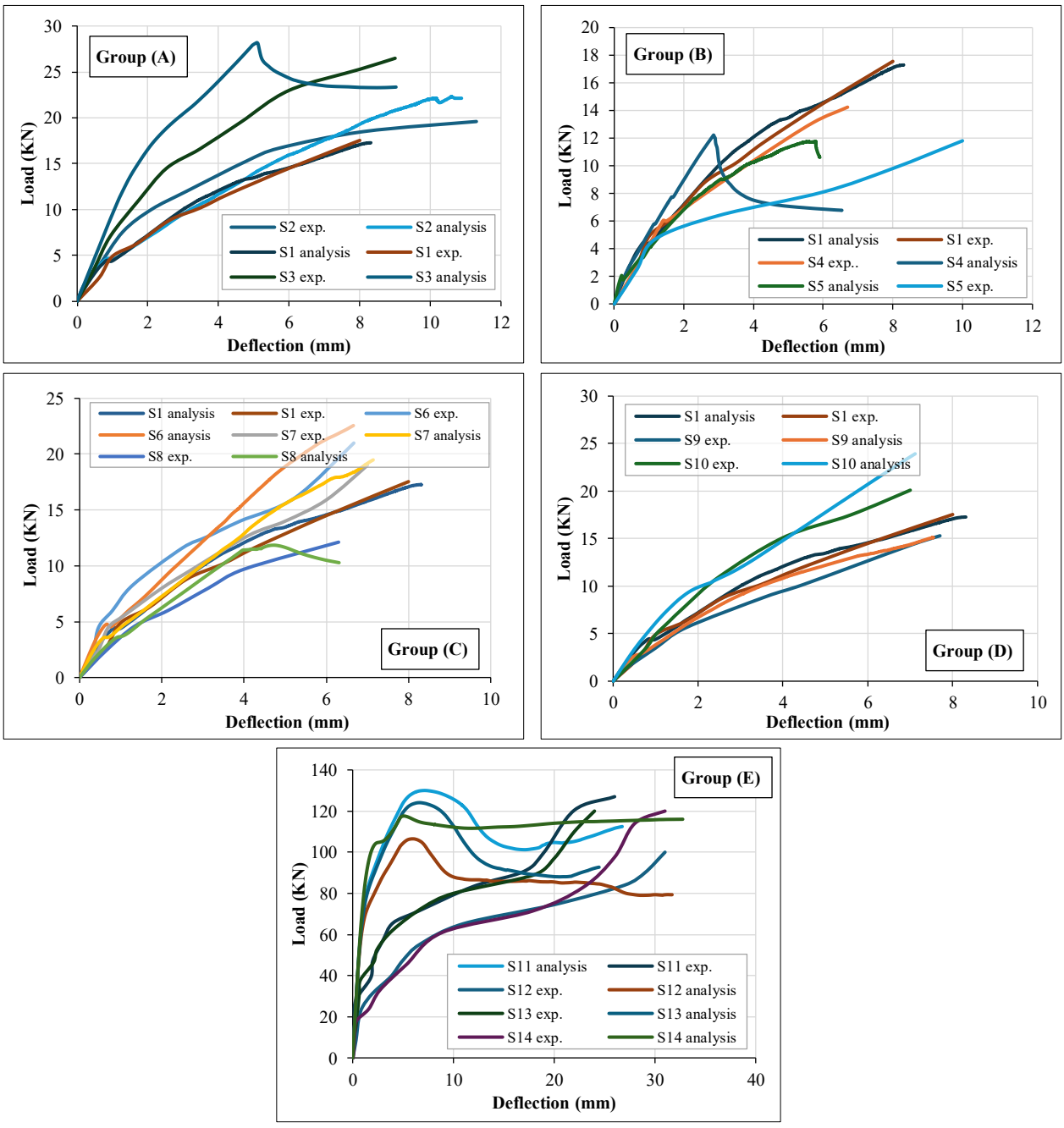

Figure 16. Comparison between load-deflection curves of experimental and numerical analysis

6.3. Effect of Lattice Girder Height

Both test results and numerical analysis show that increasing the girder height enhances the overall flexural capacity and stiffness (Figure 16-B). The 300 mm girder slab (S5) achieved the highest ultimate load with reduced deflection at similar load levels, while the 240 mm slab (S1) displayed the lowest stiffness and earlier onset of large deflections. FEM predictions generally followed the experimental behavior, capturing the influence of girder height on stiffness and capacity, although some deviations appeared in the post-cracking stage, especially for S5. The improved performance with taller lattice girders can be attributed to the increased section depth, which raises the moment of inertia and delays yielding of the reinforcement.

6.4. Effect of Top Chord Diameter

Both the experimental data and FEM results show that increasing the top chord diameter enhances the slab's flexural capacity and stiffness (Figure 16-C). The slab with the largest diameter (S6) achieved the highest ultimate load and exhibited the smallest deflection for a given load level, indicating improved resistance to bending and delayed yielding of reinforcement. Conversely, the smallest diameter (S8) resulted in the lowest load capacity and greater deflections, reflecting reduced stiffness. FEM predictions closely followed the experimental trends, successfully capturing the beneficial effect of larger top chord diameters, though minor deviations were observed in the post-yield stage for S8. The improved performance with larger diameters is attributed to their increased cross-sectional area, which enhances tensile resistance and overall structural rigidity.

6.5. Effect of Concrete Compressive Strength

Figure (16-D) illustrates the experimental and FEM load–deflection curves for slabs with varying compressive strengths. The results demonstrate that higher concrete strength increases both the ultimate load capacity and the initial stiffness of the slabs. The 45 MPa specimen (S10) reached the highest peak load with smaller deflections at equivalent load levels, indicating enhanced resistance to cracking and delayed reinforcement yielding. In contrast, the 25 MPa specimen (S9) showed a lower ultimate load and larger deflections, reflecting reduced stiffness and earlier crack propagation. FEM predictions replicated the experimental trends with good accuracy, capturing the progressive improvement in flexural behavior as compressive strength increased.

6.6. Effect of Steel and Glass Fibers

Both experimental and FEM results confirm that incorporating steel or glass fibers significantly reduces deflection at equivalent load levels compared to the control flat slab (Figure 16-E). The glass fiber slab (S13) exhibited the smallest deflection at failure load, indicating superior crack control and stiffness improvement due to the well-distributed, high-volume fiber reinforcement. The steel fiber slab (S12) also showed enhanced performance over the plain semi-precast slab (S11), with increased load capacity and reduced deflections, though its effect on stiffness was slightly less pronounced than that of glass fibers. The FEM predictions captured these comparative trends accurately.

6.7. Measured Strain Response

Figure 17 presents a comparison of experimental and FEM-predicted strain responses at the bottom reinforcement for Group (D**)** specimens, which incorporated different types of reinforcement in the cast-in-place layer. The ABAQUS simulations accurately captured the overall behavior and strain progression across all specimens, with a particularly close match in the post-yield phase. Specimens S11 and S12, reinforced with additional steel bars and steel fibers, respectively, demonstrated enhanced stiffness and reduced strain levels relative to S13 (glass fibers) and FS28 (control flat slab). The control slab (FS28) exhibited the highest strain at ultimate load, reflecting the absence of a lattice girder mechanism. In contrast, the semi-precast slabs benefited from the truss action of the embedded steel lattice girder, which significantly mitigated stress concentrations in the bottom reinforcement. This stress reduction is attributed to the structural synergy among the truss members, enabling effective redistribution of internal forces throughout the slab depth. The close agreement between numerical and experimental results validates the FEM model's capability in capturing the complex interaction between reinforcement type, internal force transfer, and strain development, further affirming the structural efficiency of lattice-girder-reinforced semi-precast systems.

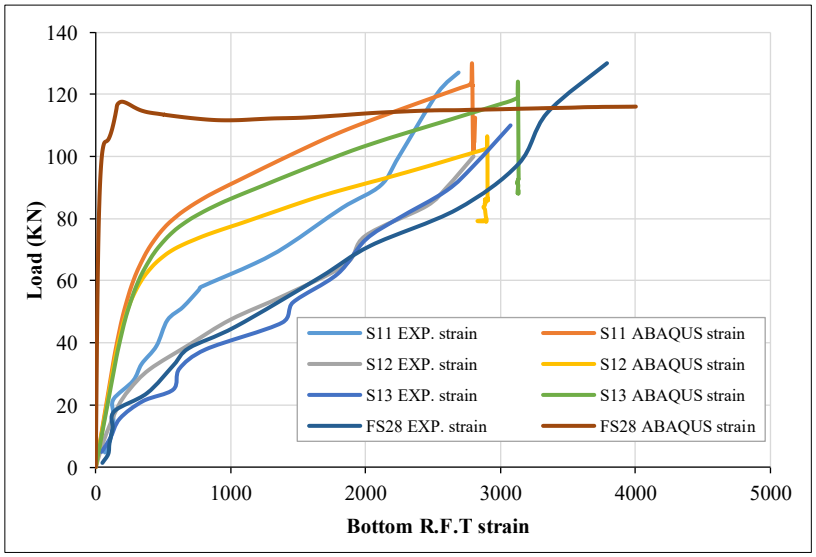

Figure 17. Load-strain curve for Group (E)

7. Conclusions

This study experimentally investigated the flexural behavior of semi-precast reinforced concrete slabs with lattice girder reinforcements under various parameters including precast slab thickness, lattice girder height, top chord diameter, concrete compressive strength, and additional reinforcement with steel and glass fibers. Based on the experimental results, the following conclusions can be drawn:

- All semi-precast slabs exhibited ductile flexural behavior, indicating their suitability for structural applications where energy dissipation and deformation capacity are critical.
- Two distinct failure modes were identified: local buckling of the top chord bar and failure at stirrup welds. The occurrence of top chord buckling before yielding stresses highlights the need for careful detailing of the lattice girder to enhance service life and safety.
- Increasing the top chord diameter and precast slab thickness significantly improved the ultimate load capacity, while increasing the lattice girder height reduced deflections, contributing to greater slab stiffness.
- The good connection between failure modes and mechanical reasoning was observed (buckling vs. welding failure), increasing the buckling significantly increasing the welding failure.
- Crack patterns observed during testing confirmed the excellent composite action between the precast slab and the cast-in-situ topping layer, a critical factor in achieving structural integrity.
- The addition of steel and glass fibers to the cast-in-situ topping showed potential benefits in enhancing crack control and serviceability; however, further optimization of fiber content and distribution is necessary for broader practical adoption.
- Semi-precast systems reduce costs by minimizing on-site labor, eliminating formwork, and accelerating construction. Based on estimates, semi-precast slabs can cut project costs by 15–25% compared to traditional cast-in-place slabs, especially in multi-unit or repetitive construction.
- Increasing the precast slab thickness and the top chord diameter significantly improved enhanced both stiffness and load capacity.
- Increasing the lattice girder height reduced slab deflection and increased stiffness.
- Thicker slabs also exhibited smaller deflections at comparable loads, indicating improved flexural rigidity.
- The higher girders improved serviceability performance by enhancing flexural rigidity.
- Larger diameters enhanced tensile resistance in the top chord, delaying yielding and reducing mid-span deflection.
- Higher-strength concrete improved the compression zone's resistance, delaying crack propagation and reducing deformation, while lower-strength concrete resulted in earlier cracking and greater deflections.
- The steel fibers increase the load-bearing capacity and crack resistance; glass fibers may offer better overall performance in reducing deflection due to their larger volume, better distribution, and crack-controlling properties.

Implications: These results support the use of semi-precast systems with lattice girders as an efficient, economical alternative to traditional slabs, especially in projects requiring accelerated construction and minimal formwork.

Limitations and Future Work: The study focused on static loading of one-way slabs. Further research should address dynamic loading, long-term durability as crack propagation and freeze-thaw, and the application to two-way or prestressed slabs.

8. Declarations

8.1. Author Contributions

Conceptualization, S.E. and W.I.; methodology, S.E. and W.I.; software, D.Y.; validation, G.G. and W.I.; formal analysis, W.I. and D.Y.; investigation, S.E. and W.I.; resources, D.Y. and G.G.; data curation, D.Y.; writing—original draft preparation, D.Y.; writing—review and editing, S.E. and W.I.; visualization, D.Y. and W.F.E.; supervision, G.G. and W.I.; project administration, S.E. and W.F.E.; funding acquisition, W.F.E. All authors have read and agreed to the published version of the manuscript.

8.2. Data Availability Statement

The data presented in this study are available in the article.

8.3. Funding and Acknowledgments

The authors confirm that the data applied in this study is primary data and were generated at the building materials laboratory of the Faculty of Engineering at Mataria, Helwan University in cooperation with the Department of Civil and Environmental Engineering in Kingdom University, Bahrain. The authors would like to acknowledge that this research work was partially financed by Kingdom University, Bahrain from the research grant number KU – 2025-2026 – 01.

8.4. Conflicts of Interest

The authors declare no conflict of interest.

9. References

[1] Abdul Kadir, M. R., Lee, W. P., Jaafar, M. S., Sapuan, S. M., & Ali, A. A. A. (2006). Construction performance comparison between conventional and industrialised building systems in Malaysia. Structural Survey, 24(5), 412–424. doi:10.1108/02630800610712004.

[2] Akmam Syed Zakaria, S., Gajendran, T., Rose, T., & Brewer, G. (2017). Contextual, structural and behavioural factors influencing the adoption of industrialised building systems: a review. Architectural Engineering and Design Management, 14(1–2), 3–26. doi:10.1080/17452007.2017.1291410.

[3] Giussani, F. B. E., & Mola, F. (2006). Precast and Cast in Situ Slab Systems for Residential Buildings. Proceedings of the 31st Conference on Our World in Concrete and Structure16-17 August, 2006, Singapore.

[4] Rasidi, N., Soehardjono, A. M. D., & Zacoeb, A. (2013). Crack width prediction in precast deck slab concrete structure. International Journal of Engineering and Technology, 3(1), 21-27.

[5] Shen, L., Tam, V. W., & Li, C. (2009). Benefit analysis on replacing in situ concreting with precast slabs for temporary construction works in pursuing sustainable construction practice. Resources, Conservation and Recycling, 53(3), 145–148. doi:10.1016/j.resconrec.2008.11.001.

[6] Pessiki, S., Prior, R., Sause, R., & Slaughter, S. (1995). Review of existing precast concrete gravity load floor framing systems. PCI Journal, 40(2), 52–68. doi:10.15554/pcij.03011995.52.68.

[7] Newell, S., & Goggins, J. (2019). Experimental study of hybrid precast concrete lattice girder floor at construction stage. Structures, 20, 866–885. doi:10.1016/j.istruc.2019.06.022.

[8] Zhang, X., Li, H., Liang, S., & Zhang, H. (2021). Experimental and numerical study of lattice girder composite slabs with monolithic joint. Crystals, 11(2), 219. doi:10.3390/cryst11020219.

[9] Hillebrand, M., Sinning, A., & Hegger, J. (2024). Shear and interface shear fatigue of semi-precast slabs with lattice girders under cyclic loading. Structural Concrete, 25(6), 4895–4917. doi:10.1002/suco.202400219.

[10] Löfgren, I. (2003). Lattice Girder Elements-Investigation of Structural Behaviour and Performance Enhancements. Nordic Concrete Research, 29(29), 85–104.

[11] Xu, Q., Chen, L., Li, X., Han, C., Wang, Y. C., & Zhang, Y. (2020). Comparative experimental study of fire resistance of two-way restrained and unrestrained precast concrete composite slabs. Fire Safety Journal, 118, 103225. doi:10.1016/j.firesaf.2020.103225.

[12] Lam, S. S. E., Wong, V., & Lee, R. S. M. (2019). Bonding assessment of semi-precast slabs subjected to flexural load and differential shrinkage. Engineering Structures, 187, 25–33. doi:10.1016/j.engstruct.2019.02.029.

[13] Mohamed, M. S., Thamboo, J. A., & Jeyakaran, T. (2020). Experimental and numerical assessment of the flexural behaviour of semi-precast-reinforced concrete slabs. Advances in Structural Engineering, 23(9), 1865–1879. doi:10.1177/1369433220904011.

[14] Baran, E. (2015). Effects of cast-in-place concrete topping on flexural response of precast concrete hollow-core slabs. Engineering Structures, 98, 109–117. doi:10.1016/j.engstruct.2015.04.017.

[15] Adawi, A., Youssef, M. A., & Meshaly, M. E. (2016). Finite element modeling of the composite action between hollowcore slabs and the topping concrete. Engineering Structures, 124, 302–315. doi:10.1016/j.engstruct.2016.06.016.

[16] Hillebrand, M., Schmidt, M., Wieneke, K., Classen, M., & Hegger, J. (2021). Investigations on interface shear fatigue of semi-precast slabs with lattice girders. Applied Sciences, 11(23), 11196. doi:10.3390/app112311196.

[17] Mahmoud, M. R. I., Wang, X., Xingyu, B., Altayeb, M., Liu, S., & Moussa, A. M. A. (2024). Flexural behaviour of semi-precast slabs of fibre-reinforced concrete reinforced with prestressed basalt fibre-reinforced polymer and steel bars. Advances in Structural Engineering, 27(15), 2609–2625. doi:10.1177/13694332241276059.

[18] Rahimi Mansour, F., Abu Bakar, S., Ibrahim, I. S., Marsono, A. K., & Marabi, B. (2015). Flexural performance of a precast concrete slab with steel fiber concrete topping. Construction and Building Materials, 75, 112–120. doi:10.1016/j.conbuildmat.2014.09.112.

[19] Song, L. T., Duan, S. J., Hou, J., Tong, J. Z., Li, Q. H., & Xu, S. L. (2025). Flexural performance evaluation on precast UHTCC-concrete composite slabs. Structures, 81(110284). doi:10.1016/j.istruc.2025.110284.

[20] Putra, B. G. D., Dewi, S. M., & Wisnumurti, W. (2025). Flexural Performance of a Semi-Precast Two-Way Slab with AAC Infill and Hybrid Bamboo–Steel Reinforcement under Point Loading. Rekayasa Sipil, 19(3), 283–289. doi:10.21776/ub.rekayasasipil.2025.019.03.3.

[21] Hernández-Pérez, J., Pascual-Francisco, J., López-González, A., Jiménez-Montoya, A., & Susarrey-Huerta, O. (2025). Flexural Behavior of Concrete Slabs Reinforced with Embedded 3D Steel Trusses. Buildings, 15(13), 2144. doi:10.3390/buildings15132144.

[22] Mahmoud, M. R. I., Wang, X., Altayeb, M., Al-Shami, H. A. M., Ali, Y. M. S., & Moussa, A. M. A. (2024). Experimental and numerical study of the flexural behaviour of semi-precast slab reinforced with prestressed FRP bars. Structures, 62. doi:10.1016/j.istruc.2024.106197.

[23] Mahmoud, M. R., Wang, X., Xingyu, B., Altayeb, M., Liu, S., & Moussa, A. M. (2024). Flexural behaviour of semi-precast slabs of fibre-reinforced concrete reinforced with prestressed basalt fibre-reinforced polymer and steel bars. Advances in Structural Engineering, 27(15), 2609–2625. doi:10.1177/13694332241276059.

[24] Newell, S., Goggins, J., & Hajdukiewicz, M. (2016). Real-time monitoring to investigate structural performance of hybrid precast concrete educational buildings. Journal of Structural Integrity and Maintenance, 1(4), 147–155. doi:10.1080/24705314.2016.1240525.

[25] Zhang, M., Feng, W., Chen, K., & Li, B. (2024). Flexural Behavior of a New Precast Insulation Mortar Sandwich Panel. Applied Sciences, 14(5), 2071. doi:10.3390/app14052071.

[26] Yun, Y., Jiang, J., & Chen, P. (2022). Flexural behavior of lattice girder slabs with different connections: experimental study. Advances in Civil Engineering, 2022(1), 7722668. doi:10.1155/2022/7722668.

[27] ASTM C33/C33M-24a. (2024). Standard Specification for Concrete Aggregates. ASTM International, Pennsylvania, United States. doi:10.1520/C0033_C0033M-24A.

[28] ES 4756-1. (2013). Cement - Part 1: Composition, specifications and conformity criteria for common cements. Egyptian Standards, Cairo, Egypt. (In Arabic).

[29] EN 197-1. (2004). Composition, specifications, and conformity criteria for common cements. European Committee for Standardization, Brussels, Belgium.

[30] ASTM C1240-20. (). Standard Specification for Silica Fume Used in Cementitious Mixtures. ASTM International, Pennsylvania, United States. doi:0.1520/C1240-20.

[31] ACI 211.1-91. (2002). Standard Practice for Selecting Proportions for Normal, Heavyweight, and Mass Concrete. American Concrete Institute (ACI), Farmington Hills, United States.